engineering proceedings

Proceeding Paper

Torsional Strength of Aluminum Shapes—Circular and Rectangular Solids †

Constance Ziemian [1], Marly McClintock [2] and Ronald Ziemian [2,*]

[1] Department of Mechanical Engineering, Bucknell University, Lewisburg, PA 17837, USA; cziemian@bucknell.edu
[2] Department of Civil and Environmental Engineering, Bucknell University, Lewisburg, PA 17837, USA; msm042@bucknell.edu
* Correspondence: ziemian@bucknell.edu

† Presented at the 15th International Aluminium Conference, Québec, QC, Canada, 11–13 October 2023.

Abstract: This paper presents an experimental investigation of 6061-T6 and 5050-H32 aluminum alloy rods and bars subjected to pure torsional loading. The test plan included five sets of 6061-T6 specimens, with solid circular and rectangular cross-sections, and four sets of 5050-H32 specimens, with solid rectangular cross-sections. Each series included six specimens, for a total of 54 tests. Resulting torque and angular twist data were used to estimate the torsional stiffness and strength, including the initial yield, full yield, and ultimate strengths. Experimental results were compared with values computed using the Aluminum Association's *Specification for Aluminum Structures* (SAS) design rules. SAS provisions were found to be overly conservative, supporting the importance of investigating changes towards an ultimate strength approach that is consistent with a limit states design specification.

Keywords: aluminum alloys; torsion testing; torsional yield strength

check for updates

Citation: Ziemian, C.; McClintock, M.; Ziemian, R. Torsional Strength of Aluminum Shapes—Circular and Rectangular Solids. *Eng. Proc.* **2023**, *43*, 4. https://doi.org/10.3390/engproc2023043004

Academic Editor: Nicolas Boissonnade

Published: 12 September 2023

1. Introduction

The usage of aluminum alloys in structural applications continues to increase as a result of their favorable properties, such as high strength-to-weight and stiffness-to-weight ratios, good corrosion resistance, and high recyclability [1]. The ease with which structural members can be fabricated from aluminum alloys offers additional benefits, allowing for a wide variety of cross-sectional shapes that accommodate a range of different loading conditions. However, the absence of a yield plateau in the stress–strain relationship of these alloys, followed by post-yield strain hardening, can serve to complicate strength estimations made using current design codes [2]. As a result, experimental research is a crucial step in evaluating and understanding the behavior of aluminum alloy structural members.

The literature is rich with experimental studies of aluminum alloy structural members subjected to axial and/or flexural loading. Experimental research of aluminum alloy columns began many years ago, and it has included studies that characterize axial load capacity and ultimate strength for a variety of alloys subjected to concentric or equivalent compressive loading [3,4], as well as eccentric compressive and/or combined loadings [5,6]. Experimental investigations of the influence of cross-sectional shape on load capacity and load–displacement response have included consideration of hollow and solid circular and rectangular sections and the effect of area or wall-thicknesses of hollow rectangular and circular sections [6–10]. Furthermore, researchers have experimentally investigated the buckling response of aluminum columns with a variety of section geometries [11,12]. Experimental studies of the flexural behavior of aluminum alloy beams [13–17] have similarly examined the influence of the material (alloy), cross-section, slenderness ratio, and moment gradient on deformation, strength, and rotation capacity. In many cases, the physical testing on columns and beams has been followed by extensive numerical studies, several of which have supported the proposal to reconsider aspects of currently available design codes that appear to be overly conservative.

Experimental studies on aluminum alloy shafts subjected to torsional loading are more difficult to find in the literature, especially those specific to examining yielding as opposed to shear buckling. Wu et al. [18] conducted torsion tests on high purity aluminum (cast and extruded) in both axially free- and fixed-end restraint configurations. The series of tests examined round tubular specimens of three different gauge lengths, with inner diameter of 25.4 mm and wall thickness of 6.4 mm, and concluded that long, thick-walled specimens are suitable for torsional use in the large strain range. Bressan and Unfer [19] developed a custom torsion machine to simulate the strain rate that occurs during cold rolling, and they used it to test solid circular shafts and measure the strain sensitivity of several materials, including pure aluminum. At the present time, and to the authors' knowledge, the literature has not provided results of any significant experimental investigations into the torsional strength of solid aluminum alloy shapes.

The present experimental study examines the torsional loading of 6061-T6 and 5050-H32 aluminum alloys. Rather than focusing on thin-walled shafts for which behavior is governed by shear buckling, this study investigates full plastic yielding and ultimate strengths of solid cross-sections, as a basis towards establishing strengths beyond the initial yield. Future work will investigate thick-walled sections. Theoretical results are presented along with comparisons with data from the physical testing. This project is motivated by the need for accessible experimental results from the torsion testing of aluminum alloys, as well as the goal of improving the current design provisions for aluminum alloys subjected to torsional loading within the *Specification for Aluminum Structures* (SAS) [20] found in Part 1 of the *Aluminum Design Manual (ADM)* [21]. While the current *ADM* provides guidance to the designer with regard to circular shafts (rods), it does not consider noncircular solid sections and it only reflects initial yielding and ultimate strengths for rods. This study represents the first step towards developing improved design provisions (for circular and noncircular shafts) that are analogous to the full yield and ultimate moment capacities currently provided within the SAS provisions for flexural members.

2. Materials and Methods

The study was focused on characterizing the mechanical behavior of aluminum alloy rods and bars subjected to torsional loading. In addition to torsion testing, tensile tests were conducted in order to obtain the elastic (Young's) modulus, yield strength, and ultimate strength of the materials investigated. These properties assisted in the design of the experiments and were needed for the subsequent analysis of the torsion data.

2.1. Test Specimens

2.1.1. Materials

Tensile and torsion testing was conducted on 6061-T6 and 5050-H32 aluminum alloy specimens. The material was supplied by the manufacturer as 6061-T6 rod stock with a diameter of 19.1 mm (0.75 in), and as 12.7 mm (0.5 in) thick plate stock for both the 6061-T6 and 5050-H32 alloys.

2.1.2. Tensile Specimens

Tensile specimens were manufactured in accordance with ASTM's *Standard Test Methods for Tension of Metallic Materials* [22] from the same plate stock purchased for the torsion testing experiments. The dogbone-shaped specimen thickness was thus 12.7 mm thick and had length and width dimensions as shown in Figure 1.

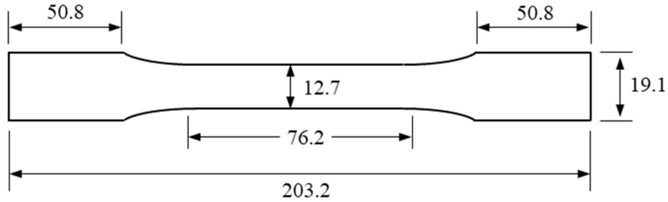

Figure 1. Tension specimen. Dimensions in mm.

2.1.3. Torsion Specimens

The torsion tests were performed on 6061-T6 circular solid section rods and 6061-T6 and 5050-H32 rectangular solid section bars. The 6061-T6 alloy rod stock (19.1 mm diameter) was cut to lengths of 457 mm (18 in). The plate stock (12.7 mm thick) for rectangular sections of both alloys was cut to the same length of 457 mm (18 in) and to a variety of widths. The test program included 54 torsion specimens, with 6 specimens in each of 9 series categorized by different combinations of alloy and section geometry. The circular series included 6 rods of 6061-T6 alloy, and the rectangular series each included 6 bar specimens per alloy (6061-T6 and 5050-H32) with widths of 12.7, 25.4, 38.1, or 50.8 mm corresponding to aspect ratios of width/thickness equal to 1, 2, 3, or 4, respectively (Table 1).

The test specimens were labeled according to their aluminum alloy, cross-section shape, and cross-section dimensions. The first two digits of the specimen label indicate the material (alloy and heat-treatment or temper), where "60" refers to the 6061-T6 aluminum and "50" refers to the 5050-H32. The second part of the label indicates the shape of the specimen cross-section, with "C" indicating circular and "R" indicating rectangular. The third part of the label is associated with the cross-sectional dimensions. For the circular specimens, "D19" indicates the nominal diameter which is 19.1 mm. For the rectangular specimens, "AR" refers to the cross-sectional aspect ratio and the number is the width/thickness, with thickness equal to 12.7 mm for all rectangular specimens.

Table 1. Description of the 9 test-series, with 6 specimens in each.

Test Series		Aluminum	Cross-Section
No.	**Label**	**Alloy**	**Dimensions (mm)**
1	60-C-D19	6061-T6	Dia = 19.1 [1]
2	60-R-AR1	6061-T6	12.7 × 12.7
3	60-R-AR2	6061-T6	12.7 × 25.4
4	60-R-AR3	6061-T6	12.7 × 38.1
5	60-R-AR4	6061-T6	12.7 × 50.8
6	50-R-AR1	5050-H32	12.7 × 12.7
7	50-R-AR2	5050-H32	12.7 × 25.4
8	50-R-AR3	5050-H32	12.7 × 38.1
9	50-R-AR4	5050-H32	12.7 × 50.8

[1] Note: 1 in. = 25.4 mm.

2.2. Test Procedures

2.2.1. Tensile Testing

Tension tests were completed on an Instron 5584 Universal Testing Machine with a load cell capacity of 200 kN. Three specimens of each alloy were tested. An extensometer was attached to the specimen with an initial separation or gauge length of 25.4 mm (Figure 2). Force and displacement data were recorded with accuracies of ±0.5%. A test speed of 5 mm/min was adopted in accordance with ASTM-E8 [22] in order to prevent rate-dependent effects.

Figure 2. Tensile testing setup.

The engineering stress and strain were respectively determined from the force–displacement data as $\sigma = P/A_o$ and $\varepsilon = (L - L_o)/L_o$, where P is the axial force of the machine, A_o is the initial cross-sectional area ($t{*}w$ = 241.9 mm^2), L_o is the original extensometer length of 25.4 mm, and L is the instantaneous extensometer length measured during the test. After converting force–displacement data to engineering stress and strain, the values of Young's modulus (E), the 0.2% offset yield stress (F_y), and the ultimate tensile stress (F_u) were determined (Table 2). In this paper, the median value of these properties will include the superscript "*tt*" to indicate that they were obtained experimentally from tension tests.

Table 2. Median values of measured material properties of tensile coupons in MPa.

Material	E^{tt}	F_y^{tt}	F_u^{tt}
6061-T6	70,300	321.0	346.7
5050-H32	69,400	135.1	209.5

2.2.2. Torsion Testing

Without an ASTM standard specifically focused on the torsion testing of circular rods or rectangular bars, ASTM A938: Torsional Testing of Wire [23] was used to guide the experimental procedures. A Tinius Olsen torsion tester with a capacity of 6800 Nm (60,000 lb-in) was used for the experiments. The machine is capable of achieving large twist angles in one test run while not restraining the axial (lengthwise) deformation of the specimen. Figure 3 shows the test setup.

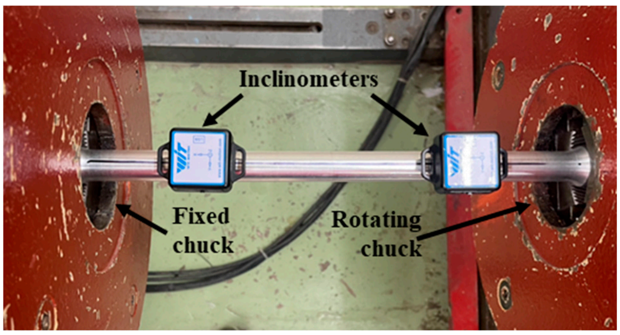

Figure 3. Top view of the torsion test setup with two inclinometers mounted on the CSS specimen.

Custom grips were used to secure each different cross-sectional geometry, and 6 specimens were tested for each series using a test speed of 0.524 rad/min. Torque and angular displacement data were recorded using wireless inclinometers (WitMotion Bluetooth 2.0), with an angle accuracy of 872.7 µrad (0.05°) for this static testing. Two inclinometers were attached to each specimen at a constant length of separation, as shown in Figure 3, and the angular rotation at each attachment point was measured every 0.1 s. Angular deformation between the two attachment points of these inclinometers was computed as the difference between the two recorded angles. A third inclinometer/sensor was used in conjunction with the load recording dial for the simultaneous collection of the applied torque. The resulting angular deformation and torque data were recorded for each specimen.

2.3. Data Analysis

The torsion test results include applied torque T and the corresponding angular deformation ϕ, for both circular and rectangular sections. The data were analyzed in order to assess torsional stiffness and the torques associated with the initial yield, full plastic yield, and ultimate strengths of each specimen.

In analyzing the circular cross-section (C) specimens as the applied torque T increases, but prior to the onset of any yielding, the shear stress distribution is known to vary linearly with respect to the radial distance ρ from the axis of rotation [24]. As a result, the maximum shear stress for a given torque T occurs at the maximum radial distance or ρ = R, which corresponds to the outer surface of the rod. When yielding begins, the initial yield will therefore occur simultaneously at all points on the outermost rod surface, and it will progress inward (ρ decreasing) as T continues to increase and yielding progresses. For the C-specimens, the shear stress at which the first yield occurs is thus:

$$\tau_y = \frac{T_y R}{J} = \frac{T_y R}{\frac{\pi R^4}{2}} = \frac{2T_y}{\pi R^3} \tag{1}$$

where the torsional constant J is the polar moment of inertia of the section. The torque at which initial yielding occurs is thus:

$$T_y = S_T \tau_y = \left(\frac{\pi R^3}{2}\right)\tau_y \tag{2}$$

where S_T is the torsional elastic section modulus, $\tau_y = 0.577\sigma_y$ per the von Mises yield criterion [24], and σ_y, which is often denoted in specifications as F_y, is the tensile yield stress of the material. Per Equations (1) and (2), $S_T = J/R$ for circular cross-sections.

As the torque continues to increase, yielding progresses inward from the outer surface of the rod until the cross-section fully yields when the torque reaches the plastic value T_p. Assuming that no strain hardening occurs at the surface of the rod, the fully plastic torque is defined as

$$T_p = \int_0^{2\pi}\int_0^R \tau_y \rho^2 \, d\theta \, d\rho = \left(\frac{2}{3}\pi R^3\right)\tau_y = Z_T \tau_y \tag{3}$$

where Z_T is the torsional plastic section modulus. Note that the convention of using S and Z is based on the analogous properties and behavior used when analyzing flexure. Extending Equation (3) from full yield to rupture, as is currently carried out in SAS for rods, the torque at ultimate, T_u, can be written in terms of the ultimate shear stress, τ_u, as

$$T_u = Z_T \tau_u \tag{4}$$

Similarly, theoretical solutions for the initial yield and full plastic yield torques for the solid rectangular sections (Figure 4) can be determined using Prandtl's membrane analogy [25] and Nadai's sand heap analogy [26], respectively.

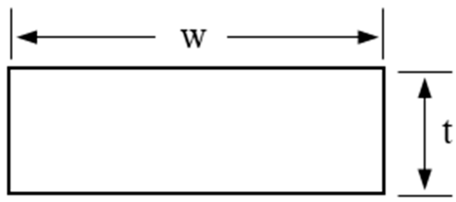

Figure 4. Cross-section shape of RSS specimens, with $t \leq w$.

The torque associated with the initial yield of a solid rectangular section (Figure 4), as derived by Ugural and Fenster [24] is

$$T_y = S_T \tau_y = \left[\left(\frac{8}{3\alpha} \right) \left(\frac{w}{2} \right) \left(\frac{t}{2} \right)^2 \right] \tau_y$$
$$\text{with } \alpha = 1 + 0.6095 \left(\frac{t}{w} \right) + 0.6685 \left(\frac{t}{w} \right)^2 - 1.8023 \left(\frac{t}{w} \right)^3 + 0.9100 \left(\frac{t}{w} \right)^4. \tag{5}$$

The torque associated with the full plastic yield of a solid rectangular section [24] is determined to be

$$T_p = Z_T \tau_y = \left[\frac{1}{6} t^2 (3w - t) \right] \tau_y \tag{6}$$

Similarly, the ultimate torque is $T_u = Z_T \tau_u$, with the torsional plastic section modulus Z_T defined in Equation (6).

3. Results and Discussion

The results of the physical testing were analyzed using the relationships presented in Equations (1)–(6).

3.1. Torsional Stiffness

The torque and angular displacement data from each test were first examined with regard to specimen stiffness in order to assess the experimental setup. A sample plot of the data is presented in Figure 5 for several rectangular specimens with an aspect ratio w/t = 3, i.e., 60-R-AR3 series.

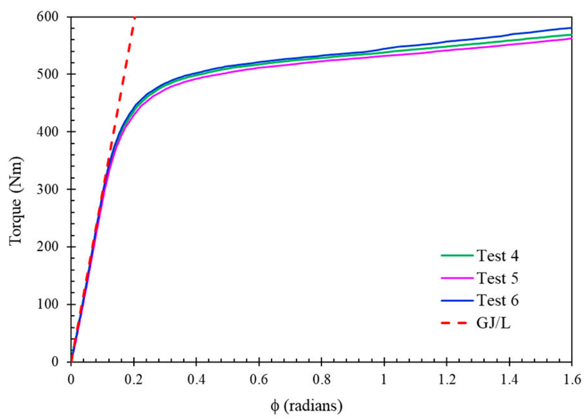

Figure 5. Representative plots of torsion results for 60-R-AR3, with the least squares regression line.

The slope of the linear elastic portion of the experimental data was determined for each test specimen using least squares regression. This value is considered to be the experimental torsional stiffness K of the specimen. In this paper, the median of the six experimental values of specimen stiffness K in a test series is referred to as the "experimental" torsional stiffness, or K^{exp}. The value of K^{exp} for each series was then compared with two different computed values of GJ/L, which will be referred to as K^{ADM} and K^{tt}, with the superscript referring to the elastic modulus used in the calculation. Both computed values used (a) the appropriate theoretical expression for the torsion constant J for the given cross-section [27],

(b) experimental gauge length L = 181.5 mm, and (c) shear modulus G from the theoretical relationship [24]

$$G = \frac{E}{2(1+\nu)} \quad (7)$$

with Poisson's ratio ν = 0.33. For K^{ADM}, the elastic modulus E was set to the recommended *ADM* table value $E^{ADM} = 70$ GPa for each alloy, and for K^{tt}, the modulus E was taken as the median of the least squares values determined from the tension tests, E^{tt} (Table 2).

For the example (60-R-AR3) presented in Figure 5, the median slope obtained from the torsion tests was K^{exp} = 2947.1, the computed K^{ADM}= 2967.6, and K^{tt}= 2992.0 Nm/rad. The percent errors in comparing the computed values to the actual experimental value were 0.70% and 1.5%, respectively. Comparisons were made for each test series and are presented in Table 3 in ratio form. The small variation observed established the validity of the test apparatus and experimental procedures.

Table 3. Comparison of computed values for specimen stiffness, *GJ/L*, with the least squares slope of the experimental torsion data.

Stiffness Ratio	60-C-D19	60-R-AR1	50-R-AR1	60-R-AR2	50-R-AR2	60-R-AR3	50-R-AR3	60-R-AR4	50-R-AR4
K^{tt}/K^{exp}	1.01	1.06	1.05	0.93	1.05	1.02	1.04	0.97	1.03
K^{ADM}/K^{exp}	1.00	0.98	1.03	0.92	1.05	1.01	1.05	0.96	1.04

3.2. Torsional Strength

Although the analysis of strength data is ongoing, the following is a sample of the results obtained to date.

3.2.1. Yield Strengths

The torque and angular displacement data were analyzed with regard to the first yield and full plastic yield strength relationships presented in Equations (2)–(6). For each test series, comparisons were made between the yield strengths determined using SAS [20] and those based upon physical tension test results. Specifically, in computing an alloy's shear yield stress τ_y for use in Equations (2)–(6), SAS prescribes τ_y = $0.6F_y^{ADM}$, where F_y^{ADM} is the specification's recommended tabular value for the material yield strength (240 MPa for 6061-T6 and 160 MPa for 5050-H32). In contrast, the tension test-based value uses τ_y = $0.577F_y^{tt}$, where 0.577 is equal to the $1/\sqrt{3}$ von Mises criterion [24], and F_y^{tt} is the median of 0.2% tensile yield strengths obtained from experimentation (Table 2). The τ_y values are then multiplied by the relevant torsional section modulus, i.e., elastic S_T or plastic Z_T, to obtain the torques (T_y and T_p respectively) associated with the initial yield and full plastic yield for each method.

A graphical representation of the comparison of these results for the 60-R-AR3 series appears in Figure 6.

The torque associated with the initial yield as determined using the experimental tension test results for the elastic modulus, T_y^{tt}, occurs at an ordinate location where the T -vs- ϕ plot begins to appear nonlinear. The associated full plastic torque T_p^{tt} is above the transition point (sometimes termed the "knuckle") at which the specimen stiffness has a decreased constant slope, indicating that strain hardening is occurring within the cross-section material. Both of these values correspond with what is expected. Given that the horizontal lines indicating T_y^{ADM} and T_p^{ADM} are based on the *ADM* recommended material strength F_y^{ADM}, which is significantly smaller than the values based on the experimental material strength F_y^{tt}, they consistently fall well below T_y^{tt} and T_p^{tt}, respectively, for all test series.

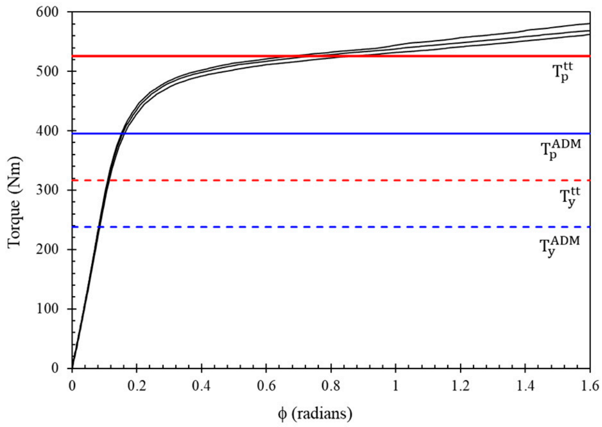

Figure 6. Representative plots of torsion results for 60-R-AR3, with the initial yield and full plastic yield torques shown for both methods.

3.2.2. Ultimate Strength

The ultimate torsional strengths were computed using Equation (4) with the appropriate torsional plastic section modulus Z_T and the relevant value for the ultimate shear stress, τ_u. Similar to the shear stress calculations, SAS prescribes $\tau_u = 0.6F_u^{ADM}$, with F_u^{ADM} equal to 290 MPa for 6061-T6 and 215 MPa for 5050-H32 and the tension test-based value used $\tau_u = 0.577F_u^{tt}$. The computed torsional ultimate strengths, T_u^{ADM} and T_u^{tt}, were then compared with the median ultimate torque values achieved during physical torsion testing, T_u^{exp}. These comparisons appear in Table 4, where the trending decrease in the ratios is evident as the width/thickness aspect ratios increase.

Table 4. Comparison of computed ultimate torques with the median experimental values.

T_u Ratios	60-C-D19	60-R-AR1	50-R-AR1	60-R-AR2	50-R-AR2	60-R-AR3	50-R-AR3	60-R-AR4	50-R-AR4
T_u^{tt} / T_u^{exp}	0.91	0.89	0.86	0.76	0.73	0.69	0.60	0.58	0.49
T_u^{ADM} / T_u^{exp}	0.76	0.75	0.88	0.64	0.75	0.57	0.61	0.49	0.50

As highlighted by the ratios in Table 4 and the extreme deformation observed before rupture occurred (Figure 7), the specimens proved to have significantly more experimental strength and ductility than may have been expected. In all cases, the specimens deformed over several full revolutions of 2π radians. It is also interesting to note that the rectangular specimens appear to withstand more angular deformation prior to rupture than the cylindrical rods. Finally, it can be seen that the T_u ratios presented in Table 4 become quite small (a minimum of 0.49) for the larger w/t aspect ratios, which is most likely attributed to the presence of warping resistance due to cross-section distortion, which is not accounted for in Equation (4).

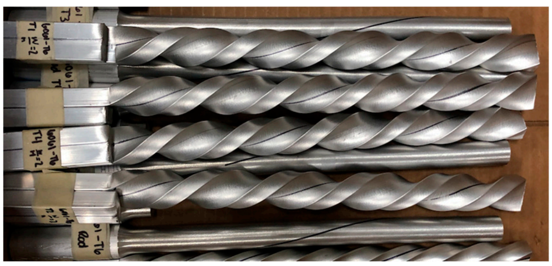

Figure 7. Sample of the 60-R-AR2 and 60-C-D19 specimens after torsion testing.

4. Summary

The results of this study support the conclusion that the design rules within the current *Specification for Aluminum Structures* [20] within the Aluminum Design Manual [21] are very conservative with regard to the torsional strength of circular shafts. This is due to the fact that SAS only considers the initial yield and ultimate torsional strengths, with the initial yield almost always controlling. In addition, the *ADM* does not include any provisions for noncircular sections subjected to torsional loading. It should be noted that when full plastic and ultimate strengths are used, as they should be in ultimate strength codes such as SAS, checks for initial yielding under service loads are highly recommended.

In order to develop improved design rules for aluminum alloy shafts, a numerical investigation is now underway. Finite element models are being developed and will be validated using the experimental results from this study. The plan for this ongoing project is to use such models to complete a parametric study of the torsional strength of shafts, which examines the effect of wall thickness for thick-walled hollow shafts with different cross-sectional shapes.

Author Contributions: Conceptualization, R.Z.; methodology, R.Z. and C.Z.; experimentation, M.M.; validation, C.Z. and M.M.; formal analysis, R.Z. and C.Z.; data curation, M.M.; writing—original draft preparation, C.Z.; writing—review and edit, C.Z. and R.Z.; funding acquisition, R.Z. All authors have read and agreed to the published version of the manuscript.

Funding: This research was funded in part by the Aluminum Association.

Institutional Review Board Statement: Not applicable.

Informed Consent Statement: Not applicable.

Data Availability Statement: The data presented in this study are available on request from the corresponding author. The data are not publicly available due to ongoing experimentation/analysis.

Acknowledgments: The support provided by the Aluminum Association is gratefully acknowledged. In addition, the authors thank Jim Gutelius for his valuable assistance with the procurement of materials, apparatus setup, and experimentation support.

Conflicts of Interest: The authors declare no conflict of interest.

References

1. Georgantzia, E.; Gkantou, M.; Kamaris, G.S. Aluminium Alloys as Structural Material: A Review of Research. *Eng. Struct.* **2021**, *227*, 111372. [CrossRef]
2. Ali, S.B.; Georgantzia, E.; Kamaris, G.S.; Gkantou, M.; Kot, P. Experimental Study of Square and Rectangular Hollow Section Aluminium Alloy Columns. In Proceedings of the 15th Global Congress on Manufacturing and Management (GCMM 2021), Liverpool, UK, 25–27 November 2020. [CrossRef]
3. Templin, R.; Strum, R.; Hartman, E.; Holt, M. *Column Strength of Various Aluminum Alloys*; Aluminum Company of America: Pittsburgh, PA, USA, 1938.
4. Hopperstad, O.S.; Langseth, M.; Tryland, T. Ultimate Strength of Aluminium Alloy Outstands in Compression: Experiments and Simplified Analysis. *Thin-Walled Struct.* **1999**, *34*, 279–294. [CrossRef]
5. Marin, J. Creep Deflections in Columns. *J. Appl. Phys.* **1947**, *18*, 103–109. [CrossRef]
6. Tsuruta, A.; Sakurai, J.; Horikawa, K. Buckling Strength of Welded Aluminium Columns. *Trans. Japan Weld. Soc.* **1972**, *3*, 285–291.
7. Clark, J.W.; Rolf, R.L. Design of Aluminum Tubular Members. *J. Struct. Div.* **1964**, *90*, 259–289. [CrossRef]
8. Zhu, J.H.; Young, B. Experimental Investigation of Aluminum Alloy Circular Hollow Section Columns. *Eng. Struct.* **2006**, *28*, 207–215. [CrossRef]
9. Zhu, J.-H.; Young, B. Tests and Design of Aluminum Alloy Compression Members. *J. Struct. Eng.* **2006**, *132*, 1096–1107. [CrossRef]
10. Zhu, J.H.; Young, B. Aluminum Alloy Tubular Columns-Part I: Finite Element Modeling and Test Verification. *Thin-Walled Struct.* **2006**, *44*, 961–968. [CrossRef]
11. Liu, M.; Zhang, L.; Wang, P.; Chang, Y. Buckling Behaviors of Section Aluminum Alloy Columns under Axial Compression. *Eng. Struct.* **2015**, *95*, 127–137. [CrossRef]
12. Zhu, J.H.; Li, Z.Q.; Su, M.N.; Young, B. Behaviour of Aluminium Alloy Plain and Lipped Channel Columns. *Thin-Walled Struct.* **2019**, *135*, 306–316. [CrossRef]
13. Kim, Y.; Pekoz, T. Ultimate Flexural Strength of Aluminum Sections. *Thin-Walled Struct.* **2010**, *48*, 857–865. [CrossRef]

14. Matteis, G.D.; Moen, L.A.; Langseth, M.; Landolfo, R.; Hopperstad, O.S.; Mazzolani, F.M. Cross-Sectional Classification for Aluminum Beams—Parametric Study. *J. Struct. Eng.* **2001**, *127*, 271–279. [CrossRef]
15. Manganiello, M.; De Matteis, G.; Landolfo, R. Inelastic Flexural Strength of Aluminium Alloys Structures. *Eng. Struct.* **2006**, *28*, 593–608. [CrossRef]
16. Su, M.N.; Young, B.; Gardner, L. Deformation-Based Design of Aluminium Alloy Beams. *Eng. Struct.* **2014**, *80*, 339–349. [CrossRef]
17. Wang, Y.Q.; Wang, Z.X.; Yin, F.X.; Yang, L.; Shi, Y.J.; Yin, J. Experimental Study and Finite Element Analysis on the Local Buckling Behavior of Aluminium Alloy Beams under Concentrated Loads. *Thin-Walled Struct.* **2016**, *105*, 44–56. [CrossRef]
18. Wu, H.-C.; Xu, Z.; Wang, P.T. Torsion test of aluminum in the large strain range. *Int. J. Plast.* **1997**, *13*, 873–892. [CrossRef]
19. Bressan, J.D.; Unfer, R.K. Construction and Validation Tests of a Torsion Test Machine. *J. Mater. Process. Technol.* **2006**, *179*, 23–29. [CrossRef]
20. Specification for Aluminum Structures (Part 1-ADM). In *Aluminum Design Manual*; Aluminum Association (AA): Washington, DC, USA, 2020.
21. Aluminum Association (AA). *Aluminum Design Manual*; Aluminum Association (AA): Washington, DC, USA, 2020.
22. *ASTM Standard E8/E8M-13a*; Standard Test Methods for Tension Testing of Metallic Materials. ASTM: West Conshohocken, PA, USA, 2013. Available online: http://www.astm.org/Standards/E8.htm (accessed on 10 July 2023).
23. *A938-07(2013)*; Standard Test Method for Torsion Testing of Wire. ASTM: West Conshohocken, PA, USA, 2015; Volume 7.
24. Ugural, A.C.; Fenster, S.K. *Advanced Mechanics of Materials and Applied Elasticity*, 6th ed.; Prentice Hall Inc.: Hoboken, NJ, USA, 2020.
25. Prandtl, L. Zur Torsion von Prismatischen Stäben. *Phys. Z* **1903**, *4*, 758–770.
26. Nadai, A. *Plasticity: A Mechanics of the Plastic State of Matter (Engineering Societies Monographs)*; McGraw-Hill: New York, NY, USA, 1931.
27. Budynas, R.G.; Sadegh, A.M. *Roark's Formulas for Stress and Strain*, 9th ed.; McGraw-Hill Education: New York, NY, USA, 1980.